

## Exchange Energy of the Ferromagnetic Electronic Ground State in a Monolayer Semiconductor

Nadine Leisgang<sup>1,2,\*</sup>, Dmitry Miserev<sup>1</sup>, Hinrich Mattiat<sup>1</sup>, Lukas Schneider<sup>1</sup>, Lukas Sponfeldner<sup>1</sup>,

Kenji Watanabe<sup>3</sup>, Takashi Taniguchi<sup>4</sup>, Martino Poggio<sup>1</sup>, and Richard J. Warburton<sup>1</sup>

<sup>1</sup>Department of Physics, University of Basel, Klingelbergstrasse 82, 4056 Basel, Switzerland

<sup>2</sup>Department of Physics, Harvard University, Cambridge, Massachusetts 02138, USA

<sup>3</sup>Research Center for Electronic and Optical Materials, National Institute for Materials Science, 1-1 Namiki, Tsukuba 305-0044, Japan

<sup>4</sup>Research Center for Materials Nanoarchitectonics, National Institute for Materials Science, 1-1 Namiki, Tsukuba 305-0044, Japan



(Received 31 October 2023; accepted 28 May 2024; published 8 July 2024)

Mobile electrons in the semiconductor monolayer MoS<sub>2</sub> form a ferromagnetic state at low temperature. The Fermi sea consists of two circles: one at the  $K$  point, the other at the  $\tilde{K}$  point, both with the same spin. Here, we present an optical experiment on gated MoS<sub>2</sub> at low electron density in which excitons are injected with known spin and valley quantum numbers. The resulting trions are identified using a model which accounts for the injection process, the formation of antisymmetrized trion states, electron-hole scattering from one valley to the other, and recombination. The results are consistent with a complete spin polarization. From the splittings between different trion states, we measure the exchange energy  $\Sigma$ , the energy required to flip a single spin within the ferromagnetic state, as well as the intervalley Coulomb exchange energy  $J$ . We determine  $\Sigma = 11.2$  meV and  $J = 5$  meV at  $n = 1.5 \times 10^{12}$  cm<sup>-2</sup> and find that  $J$  depends strongly on the electron density  $n$ .

DOI: 10.1103/PhysRevLett.133.026501

Ferromagnetism represents a state of matter in which spontaneous alignment of electron spins leads to a net magnetization. A key metric of a ferromagnet is the exchange energy  $\Sigma$ , the energy required to flip one spin.  $\Sigma$  determines the Curie temperature separating the ferromagnetic (magnetically ordered) and the paramagnetic (magnetically disordered) ground states. For metallic ferromagnets, e.g., iron,  $\Sigma$  is large,  $\sim 100$  meV, resulting in enormous Curie temperatures,  $\sim 1000$  K. The phase transition is second order.

Ferromagnetic ordering of mobile electrons has been observed in various two-dimensional (2D) systems, e.g., monolayer MoS<sub>2</sub> [1], an AlAs quantum well [2], monolayer WSe<sub>2</sub> [3], and twisted bilayer graphene [4]. As the Mermin-Wagner theorem precludes magnetic order in 2D for isotropic spins [5], magnetic anisotropy induced by a spin-orbit interaction or a small Zeeman splitting of the Fermi surfaces is required to stabilize the ferromagnetic order of a 2D electron gas (2DEG). The zero-temperature ferromagnetic phase transition controlled by the electron

density is predicted to be first order [6], an idea supported experimentally [7].

Here, we present photoluminescence (PL) with quasiresonant excitation on gated monolayer MoS<sub>2</sub> in all four polarization channels. The novelty with respect to previous experiments [1,7] lies in an interpretation of the energies of the emission lines. We first identify the emission lines one by one. We then argue that the splitting between emission lines provides a direct measurement of the ferromagnetic exchange energy  $\Sigma$ , as well as the intervalley Coulomb exchange energy  $J$ .

Monolayer MoS<sub>2</sub> is a semiconductor with direct band gaps at the  $K$  and  $\tilde{K}$  points of the Brillouin zone [8] [Fig. 1(a)]. The spin-orbit splitting is large in the valence band ( $\sim 150$  meV [9]) and small in the conduction band (a few meV [9–11]). Resonant  $\sigma^+$  polarized ( $\sigma^-$  polarized) light creates a bright exciton at the  $K$  point ( $\tilde{K}$  point). (We note that the lowest-energy excitons are dark [12,13], irrelevant here as we inject and detect bright excitons.) Recently, a pronounced optical dichroism of a 2DEG in monolayer MoS<sub>2</sub> was interpreted as ferromagnetic ordering. The Fermi surface consists of a circle at the  $K$  point and a circle at the  $\tilde{K}$  point [1]. If the spins point down, the  $K\downarrow$  and  $\tilde{K}\downarrow$  bands are occupied up to the Fermi energy; conversely, the  $K\uparrow$  and  $\tilde{K}\uparrow$  bands are pushed above the Fermi energy by the Coulomb interactions and are unoccupied [Fig. 1(b)].

Published by the American Physical Society under the terms of the Creative Commons Attribution 4.0 International license. Further distribution of this work must maintain attribution to the author(s) and the published article's title, journal citation, and DOI.

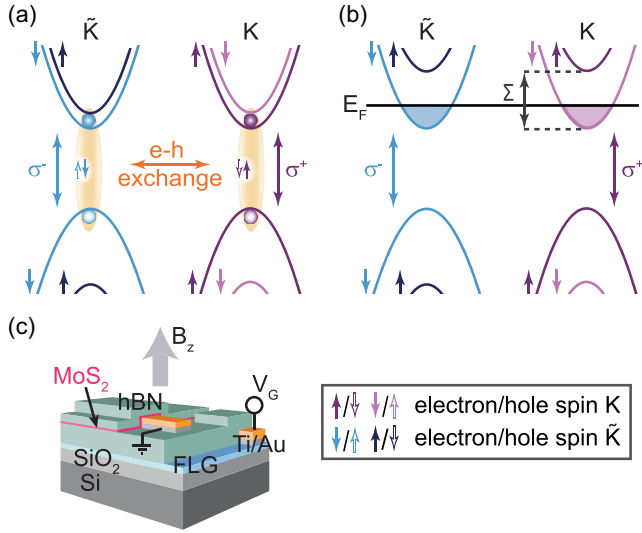


FIG. 1. (a) Band structure of monolayer MoS<sub>2</sub> showing exciton formation at the  $K$  and  $\bar{K}$  points and the intervalley scattering via electron-hole exchange. (b) Schematic of the reconstructed band structure containing ferromagnetically ordered itinerant electrons with spin  $\downarrow$ . (c) Schematic of the sample design. FLG stands for few-layer graphene.

The energy separation between the  $\uparrow$  and  $\downarrow$  bands is  $\Sigma$ , the exchange energy. The close-to-complete spin polarization implies that  $\Sigma$  is larger than the Fermi energy. The dichroism disappears rather abruptly at electron density  $n \simeq 3 \times 10^{12} \text{ cm}^{-2}$ , evidence of a first-order transition to a paramagnetic state [1]. These experimental observations are consistent with theory which predicts both spin ordering (but not valley ordering) and a first-order phase transition driven by subtle corrections to Fermi-liquid theory [6]. The goal here is to determine  $\Sigma$  at low  $n$ .

The sample consists of a MoS<sub>2</sub> monolayer sandwiched between two hBN layers [14,17,18] [Fig. 1(c)]. Electrons are injected into the monolayer via a gate electrode; the electron density  $n$  is proportional to the applied voltage, with a capacitance calculated from the device geometry. We perform a quasiresonant, quasilocal PL experiment: The laser photon energy is 1.96 eV, just above the exciton energy, 1.94 eV; the PL is collected from a region with diameter 500 nm. The laser intensity is chosen such that the steady-state exciton density is at least 2 orders of magnitude smaller than  $n$ . At these laser powers, photodoping (the influence of the laser on  $n$  via charge trapping in the environment) is both weak and slow. The remaining photodoping effects (a slight decrease in  $n$  on an hour-long timescale) are eliminated by integrating for 1200 s at one  $n$ , resetting  $n$  to zero, repeating this cycle to cover all  $n$ ; see Supplemental to Ref. [7]. This is important, as otherwise photodoping can lead to a mismatch between PL and absorption [19]. The excitation is either  $\sigma^+$  or  $\sigma^-$  polarized, thereby injecting an exciton with spin  $\uparrow$  at the  $K$  point or

spin  $\downarrow$  at the  $\bar{K}$  point, respectively. The PL is detected with  $\sigma^+$  or  $\sigma^-$  polarization. Note that, in absorption, only the eigenstates of the system are probed. A magnetic field (perpendicular to the 2DEG) of +9.00 T is applied with a direction such that only spin- $\downarrow$  bands are occupied. The optical response is plotted as a matrix (Fig. 2):  $\sigma^+/\sigma^-$  refers to excitation with  $\sigma^+$ , collection with  $\sigma^-$ , etc.

We focus initially on  $\sigma^+$  excitation. At  $n = 0$ , there is one PL line in both  $\sigma^+/\sigma^+$  and  $\sigma^+/\sigma^-$  corresponding to the neutral exciton  $X^0$ . The dichroism  $D = [I(\sigma^+) - I(\sigma^-)] / [I(\sigma^+) + I(\sigma^-)]$  is 42%. On increasing  $n$ ,  $X^0$  weakens. In  $\sigma^+/\sigma^+$ , several trions are observed, yet, in  $\sigma^+/\sigma^-$ , the PL is very weak such that  $D$  increases to  $D \simeq 64\%$  at  $n = 1.5 \times 10^{12} \text{ cm}^{-2}$ .

We propose that the increase of  $D$  at small  $n$  [up to about  $2 \times 10^{12} \text{ cm}^{-2}$ , Fig. 3(c)] is a consequence of a Bir-Aronov-Pikus electron-hole exchange. At  $n = 0$ , an exciton injected into the  $K$  valley can be scattered within its lifetime to the  $\bar{K}$  valley by the electron-hole exchange [20–22] [Fig. 1(a)]. This reduces  $D$  from the high value expected from the selection rules alone. Assuming an exciton lifetime of  $\sim 4$  ps [23,24] and that the dynamics can be described with a rate equation, the measured  $D$  implies a  $K \rightarrow \bar{K}$  scattering time of  $\sim 6$  ps (see Supplemental Material [14]), consistent with experiments in the time domain [25]. Once a Fermi surface is formed, the spin- $\downarrow$  electron states at the  $\bar{K}$  valley are occupied such that the scattering process is inhibited by the Pauli principle and  $D$  increases. This is evidence that the relevant  $K \leftrightarrow \bar{K}$  scattering mechanism is electron-hole exchange and that the  $\bar{K}\downarrow$  states become occupied.

At low  $n$ , three trions are observed in  $\sigma^+/\sigma^+$ , labeled  $T_1$ ,  $T_2$ , and  $T_3$  [Figs. 2 and 3(a)].  $T_1$  and  $T_2$  are linked: They have similar intensities and linewidths. In  $\sigma^+/\sigma^-$ , there is very weak PL from a trion, labeled  $T_4$  [Figs. 2 and 3(a)]. The energy of  $T_4$  is close to that of  $T_3$ . However, the  $n$  dependence of the  $T_3$  and  $T_4$  linewidths are quite different [Fig. 3(b)], indicating that  $T_3$  and  $T_4$  arise from different trion species.

We turn to  $\sigma^-$  excitation. Using again the trion energies and  $n$ -dependent linewidths to identify the trions, in  $\sigma^-/\sigma^+$ ,  $T_1$ ,  $T_2$ , and  $T_3$  are observed; in  $\sigma^-/\sigma^-$ ,  $T_4$  is observed. Hence, the collection channel and not the excitation channel determines which trions appear.

To proceed, we describe the trions  $T_1 \dots T_4$  microscopically (see Supplemental Material [14]). The model applies in the limit of low density where the Fermi wavelength is much larger than the trion size,  $\sim 2$  nm [26–28]. (At higher  $n$ , the eigenstates are exciton-Fermi sea polarons [1,29–32].) The low-density limit applies to the lowest  $n$  used in the experiment. The electrons have two degrees of freedom: spin  $S_z = \pm \frac{1}{2}$  and valley  $\tau_z = \pm \frac{1}{2}$  ( $+\frac{1}{2}$  for  $K$  and  $-\frac{1}{2}$  for  $\bar{K}$ ). According to the Pauli exclusion principle, the total wave function of a trion must be antisymmetric with respect to particle exchange [33,34]. The two electrons within the trion

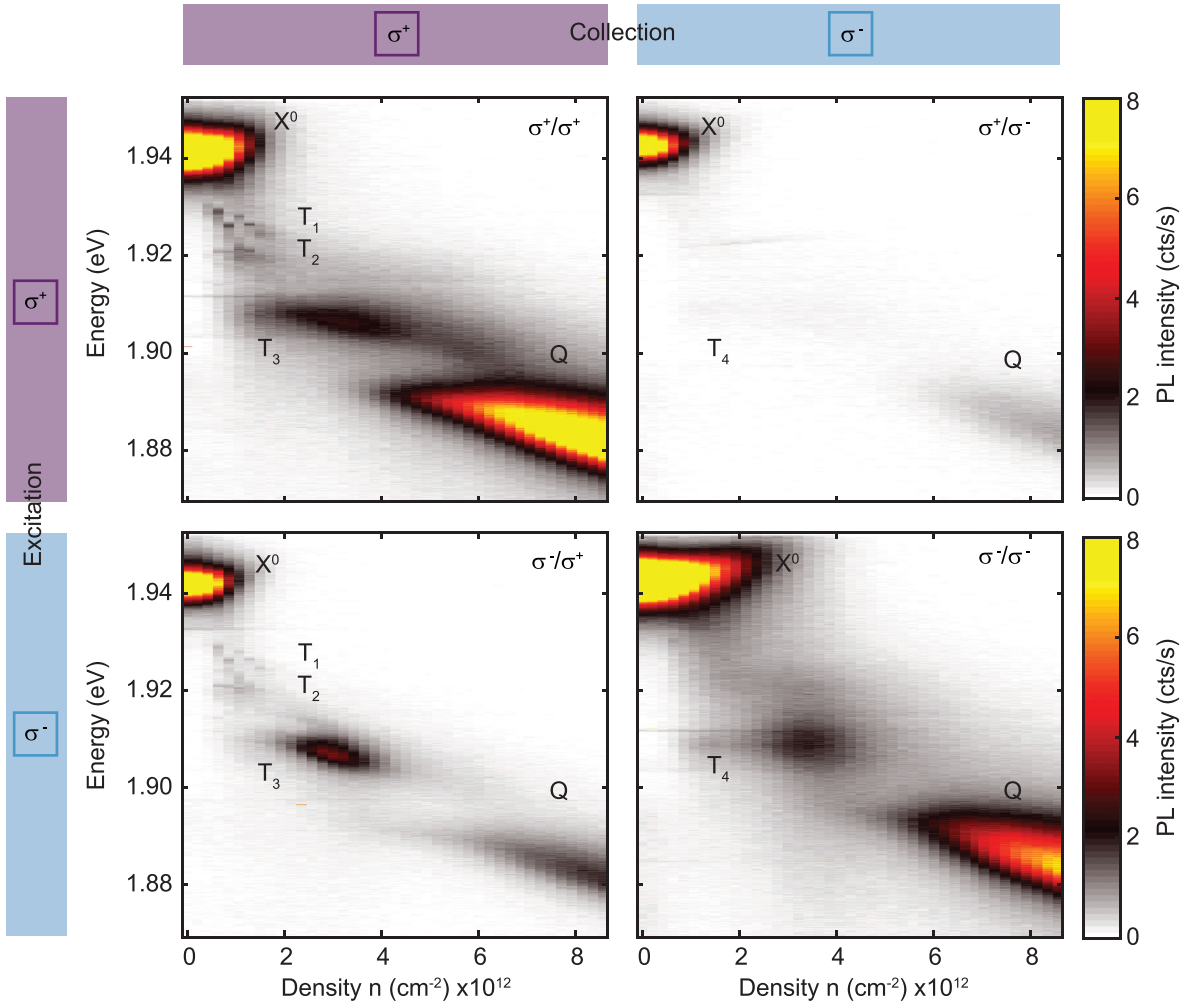


FIG. 2. PL for quasiresonant excitation on gated monolayer MoS<sub>2</sub> at +9.00 T and 4.2 K shown as a matrix: excitation in  $\sigma^+$  or  $\sigma^-$ , collection in  $\sigma^+$  or  $\sigma^-$ . Fitting of each spectrum determines the energies of all the lines.

have, therefore, six eigenstates  $|S, S_z; \tau, \tau_z\rangle$  characterized by the total spin  $S$ , its projection  $S_z$ , the valley pseudospin  $\tau$ , and its projection  $\tau_z$ . Four are relevant here:

$$\begin{aligned}
 |0, 0; 1, 1\rangle &\equiv |S_d\rangle, \\
 |0, 0; 1, 0\rangle &\equiv |S_i\rangle, \\
 |1, 0; 0, 0\rangle &\equiv |T_0\rangle, \\
 |1, -1; 0, 0\rangle &\equiv |T_-\rangle
 \end{aligned} \quad (1)$$

and are shown pictorially in Fig. 4.  $|S_d\rangle$  is the intravalley spin singlet at the  $K$  point;  $|S_i\rangle$  the intervalley spin singlet; and  $|T_0\rangle$  and  $|T_-\rangle$  are two spin components of the intervalley spin triplet.

Consider  $\sigma^+$  excitation which creates a bright exciton at the  $K$  point. The injected electron state is  $|K\uparrow\rangle$ . This electron binds with a second electron to form a trion. Binding to a second  $K\uparrow$  electron is forbidden by the Pauli principle. If the second electron is  $K\downarrow$ , the electrons form the intravalley

spin-singlet state  $|S_d\rangle$  [Eq. (1)]. The second spin can reside in the opposite valley, but only spin- $\downarrow$  electrons are available in the ferromagnetic state. The antisymmetrized state formed is  $(1/\sqrt{2})[|K_1\uparrow_1; \tilde{K}_2\downarrow_2\rangle - |K_2\uparrow_2; \tilde{K}_1\downarrow_1\rangle]$ . This state is not an eigenstate: It decomposes to  $(1/\sqrt{2})[|T_0\rangle + |S_i\rangle]$  and gives rise to two lines in the spectrum: one at the  $|T_0\rangle$  energy, the other at the  $|S_i\rangle$  energy. Under  $\sigma^+/\sigma^+$ , the lowest-energy trion  $T_3$  is thereby identified as  $|S_d\rangle$ ; the higher-energy pair,  $T_1$  and  $T_2$ , are identified as  $|S_i\rangle$  and  $|T_0\rangle$ . The model explains the observation that  $T_1$  and  $T_2$  are linked: The lines arise from recombination of the same state.

Switching to  $\sigma^-$  excitation, a bright exciton is created at the  $\tilde{K}$  point. The injected electron state is now  $\tilde{K}\downarrow$ . In the presence of only spin- $\downarrow$  electrons, the only trion that can be formed is  $|T_-\rangle$ . Under  $\sigma^-/\sigma^-$ , only  $T_4$  is observed.  $T_4$  is thereby identified as  $|T_-\rangle$ .

Finally, we analyze the cross-channels. Under  $\sigma^+/\sigma^-$ , the bright exciton at the  $K$  point is scattered to the  $\tilde{K}$  point by electron-hole exchange. Only spin- $\downarrow$  electrons are

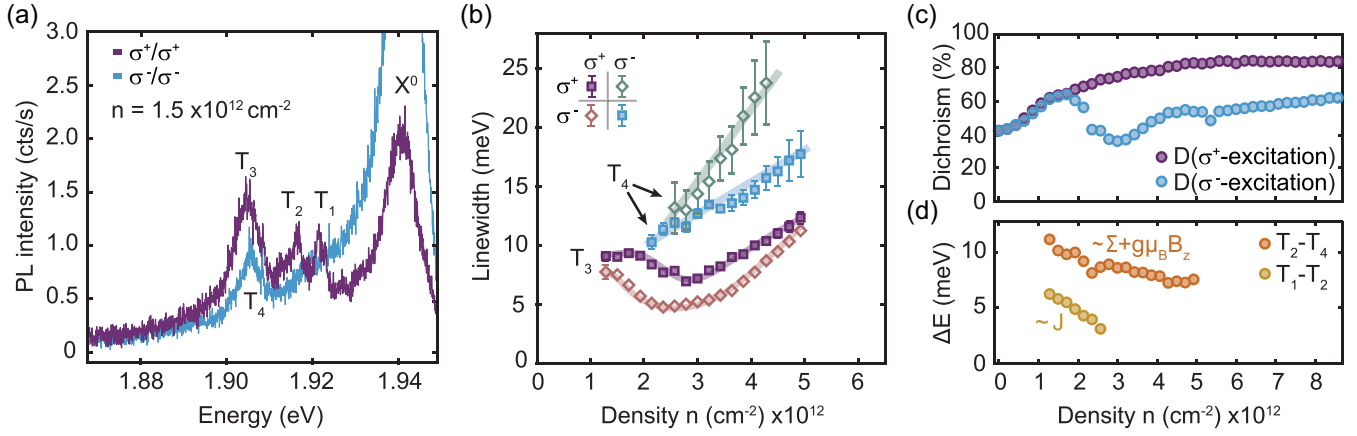


FIG. 3. (a) PL spectra at  $n = 1.5 \times 10^{12} \text{ cm}^{-2}$  (at +9.00 T and 4.2 K) for  $\sigma^+/\sigma^+$  excitation/collection and  $\sigma^-/\sigma^-$  excitation/collection. (b) Trion linewidths versus  $n$ . (c)  $n$  dependence of the optical dichroism  $D$  for  $\sigma^+$  and  $\sigma^-$  excitation. (d) Energy splitting  $\Delta E$  versus  $n$ .

available such that the only possible trion is  $|T_- \rangle$ . This is consistent with the observation of  $T_4$  in the spectrum. Under  $\sigma^-/\sigma^+$ , the bright exciton at the  $\tilde{K}$  point is scattered to the  $K$  point, making a spin- $\uparrow$  electron available, leading to the formation of  $|S_d \rangle$  and  $(1/\sqrt{2})[|T_0 \rangle + |S_i \rangle]$ , such that lines  $T_1$ ,  $T_2$ , and  $T_3$  appear in the spectrum, exactly as observed.

The model gives a consistent description of the lines in the PL matrix and is consistent with a two-band, spin- $\downarrow$  ferromagnetism. If spin- $\uparrow$  states were occupied in the Fermi sea, then a  $|S_d \rangle$ -like trion (specifically,  $|0, 0; 1, -1 \rangle$ ) would be observed under  $\sigma^-/\sigma^-$ . This is not the case. Furthermore, a doublet corresponding to  $(1/\sqrt{2})[|T_0 \rangle + |S_i \rangle]$  would be observed under  $\sigma^-/\sigma^-$ —this is also not the case. Thus, only the spin- $\downarrow$  bands in each valley are occupied.

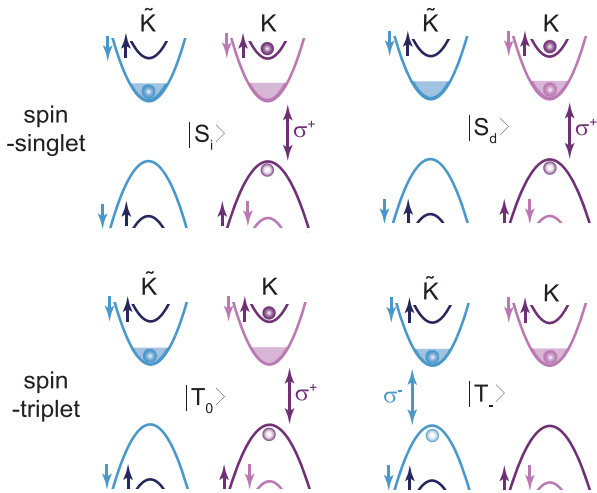


FIG. 4. Schematic of the trion eigenstates showing in each case the two electron states and the hole state from which the trion is constructed. The interpretation of the PL spectra leads to the assignment  $S_i \equiv T_1$ ,  $S_d \equiv T_3$ ,  $T_0 \equiv T_2$ , and  $T_- \equiv T_4$ .

We now consider the energies of the states (see Supplemental Material [14]), first, states  $|T_0 \rangle$  and  $|T_- \rangle$ . In a single-particle interpretation, these two states would be split by a small Zeeman energy. (Using the spin and valley  $g$  factors [10,35], the single-particle splitting between  $|T_0 \rangle$  and  $|T_- \rangle$  is  $-1.03 \text{ meV}$ .) This is not the case:  $|T_0 \rangle$  and  $|T_- \rangle$  are split by a much larger energy,  $\approx 10 \text{ meV}$ ; see Fig. 3(d). The explanation is that  $\Sigma$  contributes to  $|T_0 \rangle$  but not to  $|T_- \rangle$ . Subtracting the Zeeman splitting, we find  $\Sigma \approx 11.2 \pm 1.4 \text{ meV}$  at  $n = 1.5 \times 10^{12} \text{ cm}^{-2}$ . At this density, the Fermi energy is  $2.6 \text{ meV}$  (taking an electron mass of  $0.7m_0$  [36]), much smaller than  $\Sigma$ , as required for the consistency of Fig. 1(b).

Second, the splitting between  $|T_0 \rangle$  and  $|S_i \rangle$  arises from an intervalley Coulomb exchange interaction  $J$ , which lowers the energy of the spin-triplet  $|T_0 \rangle$  with respect to the spin-singlet  $|S_i \rangle$ , similar to Hund's rule in atoms. The splitting between  $T_1 = |S_i \rangle$  and  $T_2 = |T_0 \rangle$  provides us with  $J$  as a function of  $n$  [Fig. 3(d)]. We extract  $J \approx 5 \text{ meV}$  at  $n = 1.5 \times 10^{12} \text{ cm}^{-2}$ , indicating the importance of intervalley Coulomb exchange scattering, as pointed out in Ref. [6].

We comment on the behavior at higher  $n$ . First,  $J$ :  $J$  decreases with  $n$  [Fig. 4(d)]. The spin-down states below the Fermi energy are occupied in the ferromagnetically ordered phase such that they are excluded from the spin-down component of the trion. Conversely, the spin-up states remain unoccupied such that the spin-up component of the trion does not depend on  $n$ . The overlap between the spin-up and spin-down densities within the trion decreases with  $n$  and tends to zero at  $k_F \gg 1/a_{\text{tr}}$ , where  $a_{\text{tr}}$  is the trion size and  $k_F = \sqrt{2\pi n}$  the Fermi momentum in the ferromagnetic phase. This allows us to estimate the trion size  $a_{\text{tr}} \approx 1/\sqrt{\pi n_0} \approx 3 \text{ nm}$ , a value consistent with previous research [26–28]. Here,  $n_0 \approx 3.5 \times 10^{12} \text{ cm}^{-2}$  is the density where  $J \approx 0 \text{ meV}$  in Fig. 3(d). Second,  $\Sigma$ :  $\Sigma$  also decreases with increasing  $n$  [Fig. 3(d)]. The exchange energy of the

ferromagnetic state should decrease with increasing  $n$  as the interactions stabilizing the ferromagnetism become weaker. However, our description of the trions [Eq. (1)] is valid only at low  $n$ . At higher  $n$ , two effects potentially reduce the  $T_2$ ,  $T_4$  splitting: the dependence of exchange on density and the many-body effects on the trion energies, such that the relationship between  $\Sigma$  and the  $T_2$ ,  $T_4$  splitting is no longer clear. Our determination of  $\Sigma$  applies instead at low  $n$  where Eq. (1) is valid. Finally,  $D$ :  $D$  with  $\sigma^+$  excitation increases monotonically with  $n$ , and  $D$  with  $\sigma^-$  excitation has a dip around  $n = 3.0 \times 10^{12} \text{ cm}^{-2}$  [Fig. 3(c)]. At the highest  $n$ , the difference in  $D$  probably reflects the paramagnetism. At intermediate  $n$ , the behavior is not understood, but we note that it is determined from PL intensities which depend on many factors.

A key component of this analysis is the observation of the  $T_1 \equiv |S_i\rangle$ ,  $T_2 \equiv |T_0\rangle$  “doublet” [Fig. 3(a)] not resolved in previous experiments [1,7]. Here, smaller linewidths allowed us to resolve the doublet. The doublet is not observed at every location on the sample. Dividing a region  $6 \times 6 \mu\text{m}^2$  into pixels, the doublet is observed with a probability of 20% (see Supplemental Material [14]). There is no obvious correlation, doublet versus no doublet, with the energies, for instance, the  $X^0$  energy. It is likely that inhomogeneities result in these statistical properties.

In conclusion, we identify all the PL lines from gated monolayer  $\text{MoS}_2$ . We find that only spin- $\downarrow$  bands at each valley are occupied, signaling ferromagnetic order. At  $n = 1.5 \times 10^{12} \text{ cm}^{-2}$ , we extract from the PL spectra the ferromagnetic exchange energy  $\Sigma \approx 11.2 \pm 1.4 \text{ meV}$  and the intervalley Coulomb exchange energy  $J \approx 5 \text{ meV}$ . The large exchange energy suggests that ferromagnetic ordering should survive up to tens of degrees Kelvin. This is consistent with the observation of a pronounced dichroism even at 30 K [7]. However, at elevated temperatures, the optical probe is no longer useful on account of phonon broadening of the optical lines—this motivates an investigation with a sensitive magnetometer [37,38].

The work was supported by the Ph.D. School Quantum Computing and Quantum Technology (QCQT) of the University of Basel, the Georg H. Endress Foundation, and the Swiss Nanoscience Institute (SNI). N. L. acknowledges support from the Swiss National Science Foundation (SNF) (Project No. P500PT\_206917). K. W. and T. T. acknowledge support from the Japan Society for the Promotion of Science (JSPS) KAKENHI (Grant No. 21H05233 and No. 23H02052) and World Premier International Research Center Initiative (WPI), MEXT, Japan.

\*Corresponding author: nleisgang@g.harvard.edu

[1] J. G. Roch, G. Froehlicher, N. Leisgang, P. Makk, K. Watanabe, T. Taniguchi, and R. J. Warburton, Spin-polarized electrons in monolayer  $\text{MoS}_2$ , *Nat. Nanotechnol.* **14**, 432 (2019).

[2] M. S. Hossain, T. Zhao, S. Pu, M. A. Mueed, M. K. Ma, K. A. Villegas Rosales, Y. J. Chung, L. N. Pfeiffer, K. W. West, K. W. Baldwin, J. K. Jain, and M. Shayegan, Bloch ferromagnetism of composite fermions, *Nat. Phys.* **17**, 48 (2021).

[3] K. Hao, R. Shreiner, A. Kindseth, and A. A. High, Optically controllable magnetism in atomically thin semiconductors, *Sci. Adv.* **8**, eabq7650 (2022).

[4] A. L. Sharpe, E. J. Fox, A. W. Barnard, J. Finney, K. Watanabe, T. Taniguchi, M. A. Kastner, and D. Goldhaber-Gordon, Emergent ferromagnetism near three-quarters filling in twisted bilayer graphene, *Science* **365**, 605 (2019).

[5] N. D. Mermin and H. Wagner, Absence of ferromagnetism or antiferromagnetism in one- or two-dimensional isotropic Heisenberg models, *Phys. Rev. Lett.* **17**, 1133 (1966).

[6] D. Miserev, J. Klinovaja, and D. Loss, Exchange intervalley scattering and magnetic phase diagram of transition metal dichalcogenide monolayers, *Phys. Rev. B* **100**, 014428 (2019).

[7] J. G. Roch, D. Miserev, G. Froehlicher, N. Leisgang, L. Sponfeldner, K. Watanabe, T. Taniguchi, J. Klinovaja, D. Loss, and R. J. Warburton, First-order magnetic phase transition of mobile electrons in monolayer  $\text{MoS}_2$ , *Phys. Rev. Lett.* **124**, 187602 (2020).

[8] K. F. Mak, C. Lee, J. Hone, J. Shan, and T. F. Heinz, Atomically thin  $\text{MoS}_2$ : A new direct-gap semiconductor, *Phys. Rev. Lett.* **105**, 136805 (2010).

[9] G.-B. Liu, W.-Y. Shan, Y. Yao, W. Yao, and D. Xiao, Three-band tight-binding model for monolayers of group-VIB transition metal dichalcogenides, *Phys. Rev. B* **88**, 085433 (2013).

[10] A. Kormányos, V. Zólyomi, N. D. Drummond, and G. Burkard, Spin-orbit coupling, quantum dots, and qubits in monolayer transition metal dichalcogenides, *Phys. Rev. X* **4**, 011034 (2014).

[11] K. Marinov, A. Avsar, K. Watanabe, T. Taniguchi, and A. Kis, Resolving the spin splitting in the conduction band of monolayer  $\text{MoS}_2$ , *Nat. Commun.* **8**, 1938 (2017).

[12] C. Robert, B. Han, P. Kapuscinski, A. Delhomme, C. Faugeras, T. Amand, M. R. Molas, M. Bartos, K. Watanabe, T. Taniguchi, B. Urbaszek, M. Potemski, and X. Marie, Measurement of the spin-forbidden dark excitons in  $\text{MoS}_2$  and  $\text{MoSe}_2$  monolayers, *Nat. Commun.* **11**, 4037 (2020).

[13] J. Jadczyk, J. Kutrowska-Girzycka, M. Bieniek, T. Kazimierzczuk, P. Kossacki, J. J. Schindler, J. Debus, K. Watanabe, T. Taniguchi, C. H. Ho, A. Wójs, P. Hawrylak, and L. Bryja, Probing negatively charged and neutral excitons in  $\text{MoS}_2/\text{hBN}$  and  $\text{hBN}/\text{MoS}_2/\text{hBN}$  van der Waals heterostructures, *Nanotechnology* **32**, 145717 (2021).

[14] See Supplemental Material at <http://link.aps.org/supplemental/10.1103/PhysRevLett.133.026501>, which includes Refs. [15,16], for additional information about the experimental methods and a detailed description of the theory.

[15] T. Taniguchi and K. Watanabe, Synthesis of high-purity boron nitride single crystals under high pressure by using Ba–BN solvent, *J. Cryst. Growth* **303**, 525 (2007).

[16] A. Laturia, M. L. V. d. Put, and W. G. Vandenberghe, Dielectric properties of hexagonal boron nitride and transition metal dichalcogenides: From monolayer to bulk, *npj 2D Mater. Appl.* **2**, 6 (2018).

- [17] F. Cadiz, E. Courtade, C. Robert, G. Wang, Y. Shen, H. Cai, T. Taniguchi, K. Watanabe, H. Carrere, D. Lagarde, M. Manca, T. Amand, P. Renucci, S. Tongay, X. Marie, and B. Urbaszek, Excitonic linewidth approaching the homogeneous limit in MoS<sub>2</sub>-based van der Waals heterostructures, *Phys. Rev. X* **7**, 021026 (2017).
- [18] O. A. Ajayi, J. V. Ardelean, G. D. Shepard, J. Wang, A. Antony, T. Taniguchi, K. Watanabe, T. F. Heniz, S. Strauf, X.-Y. Zhu, and J. C. Hone, Approaching the intrinsic photoluminescence linewidth in transition metal dichalcogenide monolayers, *2D Mater.* **4**, 031011 (2017).
- [19] M. Grzeszczyk, K. Olkowska-Pucko, K. Nogajewski, K. Watanabe, T. Taniguchi, P. Kossacki, A. Babiński, and M. R. Molas, Exposing the trion's fine structure by controlling the carrier concentration in hBN-encapsulated MoS<sub>2</sub>, *Nanoscale* **13**, 18726 (2021).
- [20] T. Yu and M. W. Wu, Valley depolarization due to intervalley and intravalley electron-hole exchange interactions in monolayer MoS<sub>2</sub>, *Phys. Rev. B* **89**, 205303 (2014).
- [21] M. M. Glazov, T. Amand, X. Marie, D. Lagarde, L. Bouet, and B. Urbaszek, Exciton fine structure and spin decoherence in monolayers of transition metal dichalcogenides, *Phys. Rev. B* **89**, 201302(R) (2014).
- [22] H. Yu, X. Cui, X. Xu, and W. Yao, Valley excitons in two-dimensional semiconductors, *Natl. Sci. Rev.* **2**, 57 (2015).
- [23] F. Cadiz, S. Tricard, M. Gay, D. Lagarde, G. Wang, C. Robert, P. Renucci, B. Urbaszek, and X. Marie, Well separated trion and neutral excitons on superacid treated MoS<sub>2</sub> monolayers, *Appl. Phys. Lett.* **108**, 251106 (2016).
- [24] T. Korn, S. Heydrich, M. Hirmer, J. Schmutzler, and C. Schüller, Low-temperature photocarrier dynamics in monolayer MoS<sub>2</sub>, *Appl. Phys. Lett.* **99**, 102109 (2011).
- [25] C. Mai, A. Barrette, Y. Yu, Y. G. Semenov, K. W. Kim, L. Cao, and K. Gundogdu, Many-body effects in valleytronics: Direct measurement of valley lifetimes in single-layer MoS<sub>2</sub>, *Nano Lett.* **14**, 202 (2014).
- [26] C. Zhang, H. Wang, W. Chan, C. Manolatu, and F. Rana, Absorption of light by excitons and trions in monolayers of metal dichalcogenide MoS<sub>2</sub>: Experiments and theory, *Phys. Rev. B* **89**, 205436 (2014).
- [27] J. W. Christopher, B. B. Goldberg, and A. K. Swan, Long tailed trions in monolayer MoS<sub>2</sub>: Temperature dependent asymmetry and resulting red-shift of trion photoluminescence spectra, *Sci. Rep.* **7**, 14062 (2017).
- [28] F. Rana, O. Koksai, and C. Manolatu, Many-body theory of the optical conductivity of excitons and trions in two-dimensional materials, *Phys. Rev. B* **102**, 085304 (2020).
- [29] R. Suris, V. Kochereshko, G. Astakhov, D. Yakovlev, W. Ossau, J. Nürnberger, W. Faschinger, G. Landwehr, T. Wojtowicz, G. Karczewski, and J. Kossut, Excitons and trions modified by interaction with a two-dimensional electron gas, *Phys. Status Solidi (b)* **227**, 343 (2001).
- [30] M. Sidler, P. Back, O. Cotlet, A. Srivastava, T. Fink, M. Kroner, E. Demler, and A. Imamoglu, Fermi polaron-polaritons in charge-tunable atomically thin semiconductors, *Nat. Phys.* **13**, 255 (2017).
- [31] D. K. Efimkin and A. H. MacDonald, Many-body theory of trion absorption features in two-dimensional semiconductors, *Phys. Rev. B* **95**, 035417 (2017).
- [32] M. M. Glazov, Optical properties of charged excitons in two-dimensional semiconductors, *J. Chem. Phys.* **153**, 034703 (2020).
- [33] Y. V. Zhumagulov, A. Vagov, D. R. Gulevich, P. E. Faria Junior, and V. Perebeinos, Trion induced photoluminescence of a doped MoS<sub>2</sub> monolayer, *J. Chem. Phys.* **153**, 044132 (2020).
- [34] J. Klein, M. Florian, A. Hötger, A. Steinhoff, A. Delhomme, T. Taniguchi, K. Watanabe, F. Jahnke, A. W. Holleitner, M. Potemski, C. Faugeras, A. V. Stier, and J. J. Finley, Trions in MoS<sub>2</sub> are quantum superpositions of intra- and intervalley spin states, *Phys. Rev. B* **105**, L041302 (2022).
- [35] P. E. Faria Junior, K. Zollner, T. Woźniak, M. Kurpas, M. Gmitra, and J. Fabian, First-principles insights into the spin-valley physics of strained transition metal dichalcogenides monolayers, *New J. Phys.* **24**, 083004 (2022).
- [36] R. Pisoni, A. Kormányos, M. Brooks, Z. Lei, P. Back, M. Eich, H. Overweg, Y. Lee, P. Rickhaus, K. Watanabe, T. Taniguchi, A. Imamoglu, G. Burkard, T. Ihn, and K. Ensslin, Interactions and magnetotransport through spin-valley coupled Landau levels in monolayer MoS<sub>2</sub>, *Phys. Rev. Lett.* **121**, 247701 (2018).
- [37] H. Mattiat, N. Rossi, B. Gross, J. Pablo-Navarro, C. Magén, R. Badea, J. Berezovsky, J. M. De Teresa, and M. Poggio, Nanowire magnetic force sensors fabricated by focused-electron-beam-induced deposition, *Phys. Rev. Appl.* **13**, 044043 (2020).
- [38] E. Marchiori, L. Ceccarelli, N. Rossi, L. Lorenzelli, C. L. Degen, and M. Poggio, Nanoscale magnetic field imaging for 2D materials, *Nat. Rev. Phys.* **4**, 49 (2022).